# Microdomain Orientation of PS-*b*-PMMA by Controlled Interfacial Interactions

**Sujin Ham,[†] Changhak Shin,[†] Eunhye Kim,[†] Du Yeol Ryu,\*,[†] Unyong Jeong,[‡] Thomas P. Russell,[§] and Craig J. Hawker[ǁ]**

*Department of Chemical Engineering and Department of Materials Science and Engineering, Yonsei University, Seoul 120-749, Korea; Department of Polymer Science & Engineering, University of Massachusetts, Amherst, Massachusetts 01003; and Material Research Laboratory and Departments of Materials, Chemistry and Biochemistry, University of California, Santa Barbara, California 93016*

*Received April 1, 2008; Revised Manuscript Received June 30, 2008*

ABSTRACT: The microdomain orientation in thin films of cylinder- and lamella-forming diblock copolymers, polystyrene-*block*-poly(methyl methacrylate) (PS-*b*-PMMA), was investigated as a function of the film thickness and the composition of random copolymers composed of styrene (S) and methyl methacrylate (MMA), denoted as P(S-*r*-MMA), that were anchored to the substrate. Using scanning force microscopy (SFM) and grazing incidence small-angle X-ray scattering (GISAXS), the dependence of the microdomain orientation on film thickness around lattice period (or *d*-spacing, $L_0$), where the microdomain orientations normal to the film surface could be achieved, showed that the optimal condition for the balanced interfacial interactions (the so-called neutrality in random copolymer) was 0.64 of PS mole fraction ($X_{PS}$) for the cylindrical microdomain having narrow compositional range of P(S-*r*-MMA) from 0.52 to 0.72 of $X_{PS}$, whereas for the lamella microdomain it was observed at $X_{PS} = 0.55$ ranging extensively from 0.48 to 0.78.

## Introduction

Nanoscale periodic patterns derived from block copolymer self-assembly have recently found both commercial and academic interest as precursors for nanolithographic templates,[1,2] vertical magnetic data storage,[3] nanowire fabrication,[4] and nanoporous membranes.[5] A driving force for this interest is the high degree of control over microdomain structures of block copolymers through changes in the molecular weight (*N*), volume fraction (Φ) of the components, and segmental interaction (χ), resulting in lamellar, cylindrical, gyroid, and spherical structures, tens of characteristic sizes.[6−8]

A significant challenge in diblock copolymer films is the difference in behavior for thin films when interfacial interactions can influence the orientation and ordering of the microdomains.[9,10] Especially for cylinder- or lamella-forming block copolymers, a strong preferential interaction on the substrate or a lower surface energy of one block component leads to an orientation of microdomains parallel to the film suface.[11−15] It has been also reported that the structure of self-assembled monolayers (SAMs) of alkylsiloxanes on SiOx/Si substrate plays an important role in determining the wetting behavior of block copolymer thin films, which can be correlated to the interfacial and surface energies.[16,17]

For some commercial applications, the directed self-assembly of block copolymers leading to an perpendicular microdomain orientation in thin films is desired[13,18−21] since this enables the use of the microdomain patterns as templates and scaffolds for nanolithographic applications.[22,23] This strategy has been achieved by surface modification,[24,25] strong electric field,[26,27] and solvent annealing.[28,29] Potentially the most robust of these strategies is surface modification via a neutral or nonpreferential wetting of the substrate, enabling A-*b*-B block copolymer to promote microdomain orientation perpendicular to the film surface by

the balanced interfacial interaction, which is precisely tunable by the relative composition of A-*r*-B random copolymer on the substrate.[25,30−32] By varying the composition of the random copolymers, surface properties ranging from PS to PMMA characteristics were observed from the dewetting behaviors of PS and PMMA, resulting that the interfacial energies on the substrate were balanced at an approximate styrene fraction of 0.58 in the P(S-*r*-MMA). This corresponds to the surface neutrality obtained from the dewetting experiments by homopolymers such as PS and PMMA, which has been believed to allow both lamellar and cylindrical microdomains of PS-*b*-PMMA to orient normal to the film surface.[24,33]

Recent studies on accelerated strategies for producing surface neutrality have shown that cross-linkable benzocyclobutene (BCB)-functionalized random copolymers with S and MMA, P(S-*r*-BCB-*r*-MMA)s, offer a number of advantages such as rapid processability, resistance to solvents, and substrate independence as a generalized approach to the balanced interfacial interactions. The minimum effective thickness for thermally cross-linkable thin film of P(S-*r*-BCB-*r*-MMA) was observed to be ∼5.5 nm, which prevents penetration of polymer chains to the underlying substrate.[25,32]

Here, we investigated the microdomain orientations of cylinder- and lamella-forming PS-*b*-PMMAs by tuning the surface properties depending upon the relative compositions of P(S-*r*-MMA) ranging from 0.34 of PS mole fraction to 0.85. From the dependence of the microdomain orientation on film thickness (hereafter denoted as thickness window) around $L_0$, the equilibrium period of the microdomain morphology, and the interfacially balanced compositions of the random copolymers on the substrate, the so-called neutral compositions were examined to quantitatively optimize the condition of neutrality for both the lamellar and cylindrical microdomain morphologies and to determine whether the optimal condition was the same for both morphologies. This study suggests a simple and informative guide to the thickness dependence of the perpendicular microdomain orientation of PS-*b*-PMMA by controlling the surface properties in addition to the prior efforts to control over the microdomain orientation.

* To whom correspondence should be addressed: E-mail: dyryu@yonsei.ac.kr.
[†] Department of Chemical Engineering, Yonsei University.
[‡] Department of Materials Science and Engineering, Yonsei University.
[§] University of Massachusetts.
[ǁ] University of California, Santa Barbara.

**Table 1. Characteristics of HO-Functionalized Random Copolymers Composed of S and MMA Used in This Study**

| sample code[a] | mole fraction of PS[b] | vol fraction of PS[c] | description[d] |
|---|---|---|---|
| **R34** | 0.33$^8$ | 0.37$^5$ | |
| **R48** | 0.48$^4$ | 0.52$^4$ | |
| **R52** | 0.52$^4$ | 0.56$^4$ | |
| **R55** | 0.55$^2$ | 0.59$^1$ | |
| **R57** | 0.57$^0$ | 0.60$^9$ | 59/41 (wt) of R52/R64 |
| **R59** | 0.58$^8$ | 0.62$^6$ | 37/73 (wt) of R52/R62 |
| **R61** | 0.61$^3$ | 0.65$^0$ | 20/80 (wt) of R52/R64 |
| **R62** | 0.62$^1$ | 0.65$^8$ | |
| **R64** | 0.63$^5$ | 0.67$^1$ | |
| **R66** | 0.65$^7$ | 0.69$^2$ | 50/50 (wt) of R62/R69 |
| **R69** | 0.69$^3$ | 0.72$^6$ | |
| **R72** | 0.71$^5$ | 0.74$^6$ | |
| **R78** | 0.78$^0$ | 0.80$^6$ | 50/50 (wt) of R72/R85 |
| **R85** | 0.84$^5$ | 0.86$^5$ | |

[a] P(S-*r*-MMA)s were synthesized by living free radical polymerization, having a number-average molecular weight ($M_n$) of approximately 10 000 and a polydispersity index (PDI) of less than 1.30 measured by size-exclusion chromatography (SEC). [b] Mole fractions of PS were measured by $^1$H nuclear magnetic resonance ($^1$H NMR). [c] Volume fractions of PS were calculated with mass densities of two components (1.05 and 1.184 g/cm$^3$ for PS and PMMA, respectively). [d] Samples were prepared by the solution blending between two random copolymers.

## Experimental Section

Random copolymers composed of styrene (S) and methyl methacrylate (MMA), denoted as P(S-*r*-MMA), were synthesized by nitroxide-mediated, living free radical polymerization.[33,34] Number-average molecular weights ($M_n$) and polydispersity ($M_w/M_n$) of P(S-*r*-MMA)s were approximately 10 000 and less than 1.30, respectively, as measured by size exclusion chromatography (SEC) with PS standards. Two cylinder- and lamella-forming PS-*b*-PMMA copolymers were synthesized by the sequential, anionic polymerization of styrene and methyl methacrylate in tetrahydrofuran (THF) at −78 °C in the presence of LiCl (high purity, Aldrich) under purified argon using *sec*-butyllithium as an initiator. Molecular weight ($M_n$) and polydispersity, characterized by size-exclusion chromatography (SEC) with the multiangle laser light scattering (MALLS), were 88 000 and 1.04 for a cylinder-forming PS-*b*-PMMA with PS volume fraction ($\Phi_{PS}$) of 0.72 as well as 50 000 and 1.06 for a lamella-forming PS-*b*-PMMA with $\Phi_{PS}$ of 0.50, respectively. Compositions of copolymers were determined by $^1$H nuclear magnetic resonance ($^1$H NMR) with mass densities of two components (1.05 and 1.184 g/cm$^3$ for PS and PMMA), as listed in Table 1 for random copolymers.

Surface modification by random copolymers, ranging from 0.34 to 0.85 of PS mole fraction, was prepared by thermally annealing thin films on the standard Si wafer under vacuum at 170 °C, well above the glass transition temperatures ($T_g$) of both PS (100 °C) and PMMA (115 °C) for 3 days. During this process, end-functional hydroxyl groups of the random copolymers can diffuse into the substrate and react with the native oxide layer, resulting in polymer chain brushes anchored on the substrate. The brush thickness of P(S-*r*-MMA)s was measured to be ∼4.6 ± 0.2 nm by ellipsometry (SE MG-1000, Nanoview Co.) at an incidence angle of 70° after rinsing with toluene to remove the unreacted polymer chains on the substrate.

Scanning force microscopy (SFM; Dimension 3100, Digital Instrument Co.) was operated at tapping mode to examine the surface morphology of the block copolymer thin films, where PMMA microdomains of PS-*b*-PMMA appear to be relatively bright color due to viscoelastic contrast between two block components.

Grazing-incidence small-angle X-ray scattering (GISAXS) experiments were carried out at 4C2 beamline at the Pohang Accelerator Laboratory (PAL), Pohang, Korea. The operating conditions were set to a wavelength of 1.38 Å and the sample-to-detector distance of 2.5 m. The samples were mounted in vacuum chamber, and the incident angle was fixed at 0.16° or 0.18°, which are above the critical angle (0.135°) of PS-*b*-PMMA copolymer thin films. The exposure times were 10−300 s depending on the electron density contrast of thin films. 2D GISAXS patterns were recorded using a CCD detector positioned at the end of a vacuum guide tube when the X-ray beam pass through the block copolymer thin films mounted on the sample chamber under vacuum (5 × 10$^{-4}$ Torr). To enhance the X-ray contrast, the PMMA component of the PS-*b*-PMMA thin films was selectively removed with UV exposure and acetic acid treatment. Small-angle X-ray scattering (SAXS; 4C1 beamline) was used to obtain the microdomain structures of block copolymers in the bulk state.

## Results and Discussion

The free energy for thin films of diblock copolymers is composed of two main terms in principle: both the elastic free energy of the stretched block chains and the interfacial energy at the various interfaces, $F_{elastic}$ and $F_{interface}$, respectively. Free energy can be expressed by

$$F = F_{elastic} + F_{interface} \qquad (1)$$

assuming incompressibility in the strong segregation limit of relatively larger Flory interaction parameter ($\chi_{AB}$) between two block components.[35] When a block copolymer is confined in a thin film geometry, microdomain orientation is primarily determined by the second term because the first term is the same or insignificant between the perpendicular and parallel orientations of microdomains for cylinder- and lamella-forming block copolymers. The interfacial energy is presented as a function of four interfacial tension terms given by

$$F_{interface} = f(\gamma_{A,Bs}, \gamma_{A,Ba}, \gamma_{AB}, \gamma_{sa}) \qquad (2)$$

where $\gamma_{ij}$ is the interfacial tension between two components $i$ and $j$, namely block A, block B, the substrate (s), and air (a). To control interfacial interactions $\gamma_{As}$ and $\gamma_{Bs}$ can be tuned by changing the composition of the random copolymers anchored to the substrate. When $\Delta\gamma = |\gamma_{As} - \gamma_{Bs}| = 0$, interfacial interactions are balanced, and only the film thickness controls the microdomain orientation of the block copolymers. In contrast, when $\Delta\gamma$ is large, there is a preferential interaction of a block component with the substrate and the microdomains will orient parallel to the substrate. However, for nonzero values of $\Delta\gamma$ close to zero when the film thickness is incommensurate with $L_0$, the stretching imposed on the copolymer chains to maintain an orientation parallel to the surface can be sufficiently large to overcome the preferential interactions, resulting in an orientation of the microdomains normal to the film surface. Consequently, both the film thickness and $\Delta\gamma$ can be used to control the microdomain orientation of block copolymers.[36]

The strength of the interfacial interactions can be controlled by varying the composition of the random copolymer, so as to balance interfacial interactions which, for PS and PMMA, was found to occur as a composition of 58/42 (PS/PMMA) in P(S-*r*-MMA).[33] With this surface modification, both cylindrical and lamellar microdomains will orient normal to the surface over a limited film thickness window near $L_0$ thickness. However, it is not evident that the optimal conditions for surface neutrality are the same for the two different morphologies. To address this, we investigated the thickness window as a function of the composition of a random copolymer anchored to the substrate where cylindrical and lamellar microdomains orient normal to the film surface.

A library of hydroxy-functionalized random copolymers, synthesized by living free radical polymerization, is listed in Table 1 to design tunable surface properties depending on PS compositions in the P(S-*r*-MMA). During thermally annealing thin films at 170 °C, the thin films of the random copolymers with chain brushes of ∼4.6 ± 0.2 nm thick were obtained on the substrate after rinsing with toluene. The macroscopic surface properties of the modified surfaces were assessed by water
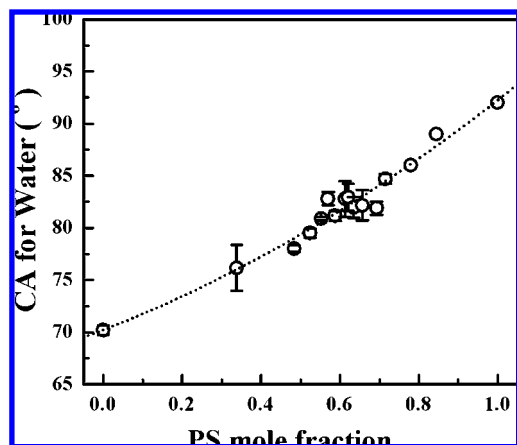
**Figure 1.** Water contact angle (WCA) for droplets on the substrates modified by random copolymers. The value increases as a second-order function with respect to the PS mole fraction ($X_{PS}$) from 70.2° for PMMA to 92.0° for PS substrates.

contact angle (WCA), as shown in Figure 1. The static WCA characterizes the relative hydrophilicity (or hydrophobicity) on the substrates since WCA for PS is higher than that of the relatively hydrophilic PMMA substrate. WCA for substrates modified by random copolymers gradually increased from 70.2° to 92.0° as the PS mole fraction ($X_{PS}$) in P(S-*r*-MMA) increased, indicating that the surface properties are well tuned by controlling the relative composition of P(S-*r*-MMA). The polynomial fit to the WCA data yields

$$WCA = 70.22 + 14.55X_{PS} + 7.48X_{PS}{}^2 \qquad (3)$$

Thin films of PS-*b*-PMMA copolymers having cylindrical microdomains of PMMA were spin-coated onto the substrates modified by various random copolymers where the thickness of PS-*b*-PMMA was varied. The indices of random copolymers, denoted as R*xy*, define the PS mole fractions of random copolymers. The scanning force microscopy (SFM) phase images for thin films of block copolymer on R64, after thermally annealing thin films at 170 °C for 24 h under vacuum, are shown in Figure 2. When the film thickness of PS-*b*-PMMA is 10 nm or thinner, the ordering of the cylindrical microdomains degrades while a partial orientation of microdomains is seen, indicating that the film thickness of PS-*b*-PMMA is insufficient to cover the entire surface. For films with thicknesses from 13 to 42 nm, the cylindrical microdomains of the PS-*b*-PMMA orient normal to the film surface due to the balanced interfacial interactions by R64. However, as the film thickness increases over 49 nm, the ordering and orientation of the cylindrical microdomains at the free surface degrades and microdomains oriented parallel to the surface are seen. This behavior can be attributed to the frustration effects arising from a commensurability between the film thickness and $L_0$. If the film thicknesses are in a vicinity of $L_0$, the microdomains orient normal to the film surface, but if the film is too thin, maintaining an orientation normal to the surface places constraints on the lateral packing of the block copolymer chains. For thicker films, since the surface energies of PS and PMMA are essentially identical at the annealing temperature, both orientations of the microdomains are possible and orientation at the surface is lost.

Detailed structural characterization of thin films for cylinder-forming PS-*b*-PMMA was conducted using grazing-incidence small-angle X-ray scattering (GISAXS) to probe the entire structure of thin films[37,38] under grazing incident angles since this is an advantageous technique for thin films of nanostructures and self-assemblies, allowing us to investigate the lateral and transverse information. Figure 3 shows GISAXS patterns of thin
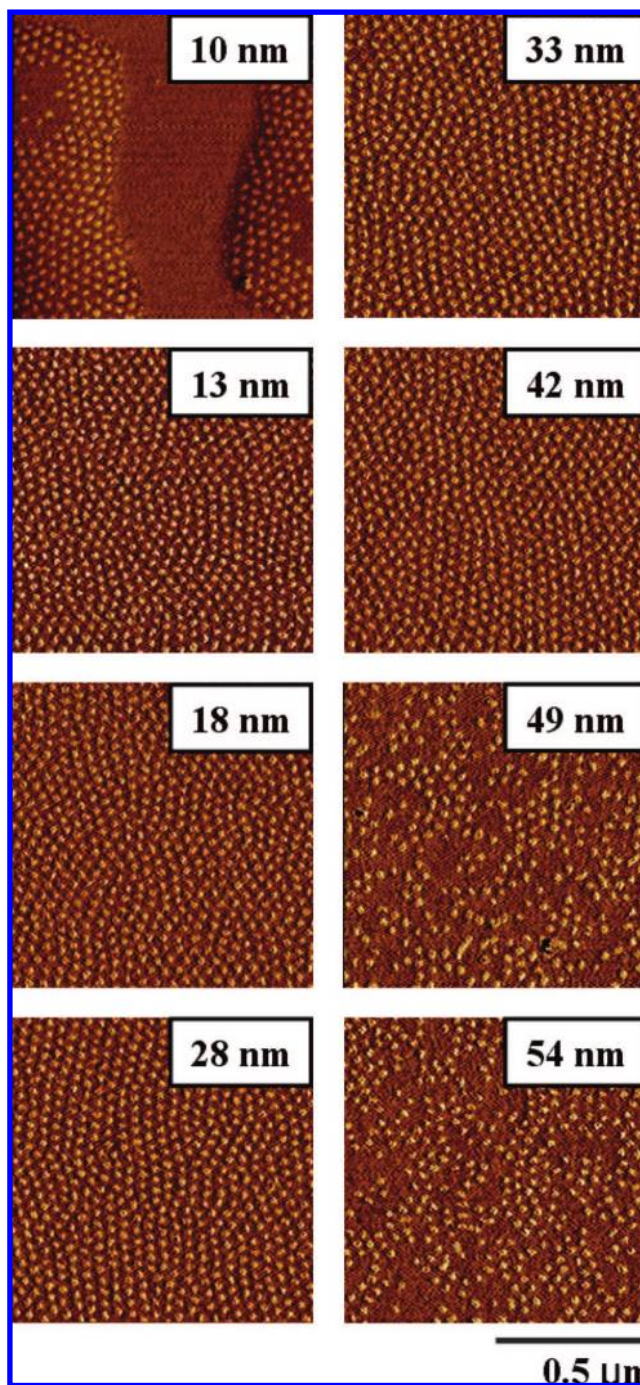


**Figure 2.** SFM phase images for thin films of cylinder-forming PS-*b*-PMMA on the substrate modified by R64 (having a PS mole fraction of 0.64) at various film thicknesses of block copolymer after thermally annealing thin films at 170 °C for 24 h.
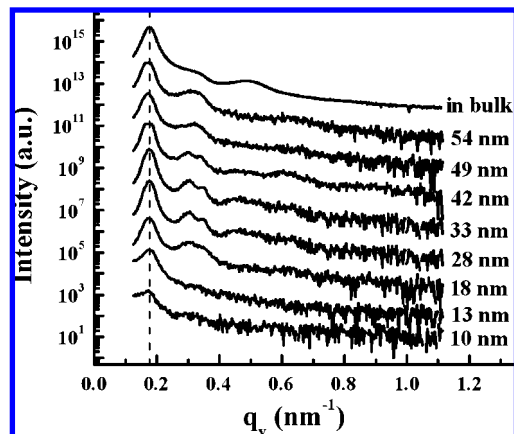
films on R64, annealed at 170 °C for 24 h followed by UV exposure and treatment with acetic acid to selectively remove the PMMA block, leaving partially cross-linked nanoporous films. The contrast for the GISAXS measurements is increased significantly for the nanoporous film. All patterns are correlated to SFM phase images (in Figure 2) for thin films on R64 with the same thicknesses. In the scattering geometry, $q_y$ is the scattering vector normal to the plane of incidence, where the $d$-spacing is related to $q_y$ by $d = 2\pi/q_y$. $q_z$ is the scattering vector normal to the sample surface, defined as $q_z = (4\pi/\lambda) \sin \theta$, where $\lambda$ is the wavelength of the X-rays and $2\theta$ is the scattering angle. Incident angles were set at 0.16° or 0.18°, which are above the critical angle (0.135°) of the films, and hence, the X-rays
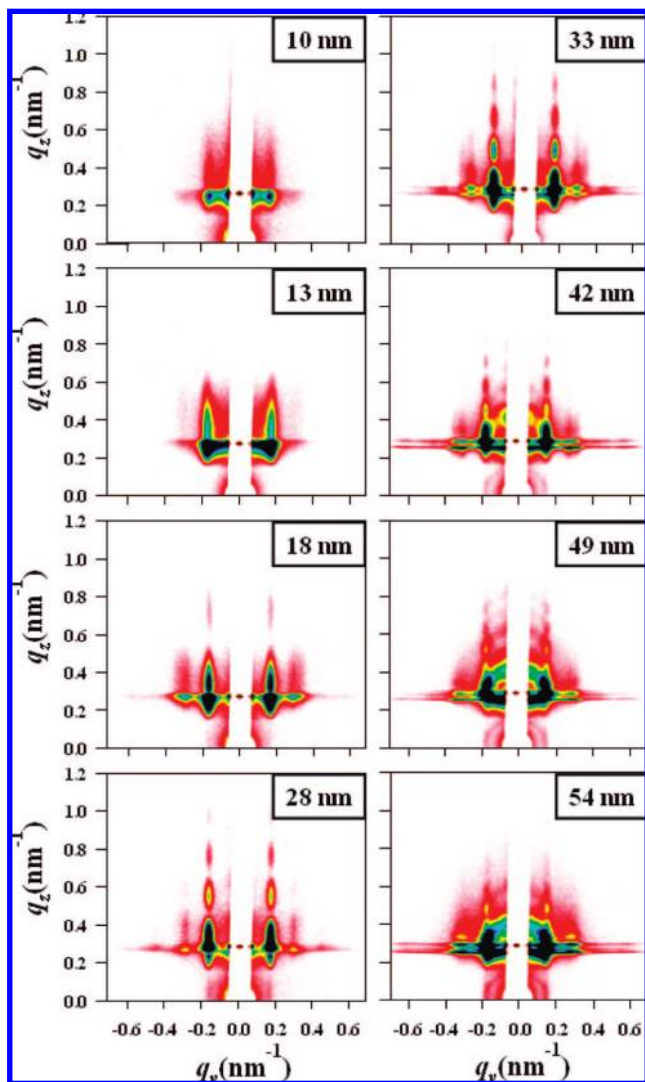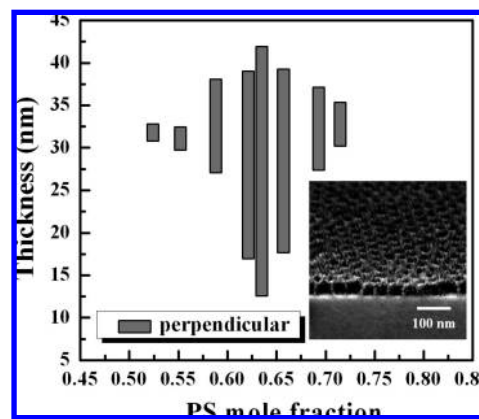
**Figure 3.** Two-dimensional GISAXS patterns at incident angles of 0.16° (10 nm thickness) and 0.18° (the others) for thin films of cylinder-forming PS-*b*-PMMA on the substrate modified by R64 at various film thicknesses of block copolymer after thermally annealing thin films at 170 °C for 24 h. To increase the scattering contrast, PMMA microdomains were removed from all thin film samples by UV exposure and subsequent rinsing with acetic acid.



**Figure 4.** Intensity profiles scanned at constant $q_z = 0.285$ nm$^{-1}$ (at $q_z = 0.254$ nm$^{-1}$ for thin film with thickness of 10 nm due to the different incident angle of 0.16°) from Figure 3 as a function of $q_y$ at various film thicknesses of block copolymer and bulk state. A dashed line is drawn to compare the peak maxima.



**Figure 5.** Thickness window for the perpendicular microdomain orientation of cylinder-forming PS-*b*-PMMA on the substrates modified by various random copolymers composed of S and MMA. The cross-sectional SEM image was taken at a tilt angle of 55° for thin film with the maximum thickness of 42 nm on R64 (having a PS mole fraction of 0.64).

penetrate the entire film probing the internal structures of the thin film.

In GISAXS patterns for thin films of block copolymer on R64, as shown in Figure 3, the scattering peaks of the 10 nm thin film show a lower intensity only for the first-order peak near $q_y = 0.177$ nm$^{-1}$ due to the degraded ordering of the cylindrical microdomains. This intensity of the first-order reflection increases, and higher-order peaks appear as the film thickness increases. GISAXS patterns for thin films with thicknesses from 13 to 42 nm, however, show a sharp first-order peak at $q_y = 0.177$ nm$^{-1}$ with higher-order peaks at a constant $q_z = 0.285$ nm$^{-1}$ at scattering vector ratios of $1:\sqrt{3}:\sqrt{4}$ relative to a first-order peak. These correspond to the scattering from hexagonally packed cylindrical microdomains oriented normal to the film surface with a *d*-spacing of 35.4 nm ($d = 2\pi/q_y$). In contrast, for thin films with thicknesses of 49 and 54 nm, GISAXS patterns reveal a ringlike scattering which arises from a random orientation of the microdomains, and the intensity at first-order reflection increases. Scattering profiles from the GISAXS patterns, scanned along the $q_y$ direction at constant $q_z = 0.254$ nm$^{-1}$ for thin film with thicknesses of 10 nm and $q_z = 0.285$

nm$^{-1}$ for the others, are shown in Figure 4 which reflect the structural changes in the entire films. Higher-order reflections are not evident for films thinner than 18 nm, but two separate shoulders at $q_y = 0.306$ and $0.350$ nm$^{-1}$ for films with thicknesses up to 42 nm, can be seen, which corresponds to the maximum thickness where a microdomain orientation normal to the film surface is observed on the surface modified by R64. In the case of thicknesses of 49 and 54 nm, the higher-order peaks merge into a broader peak due to random orientations of microdomains.
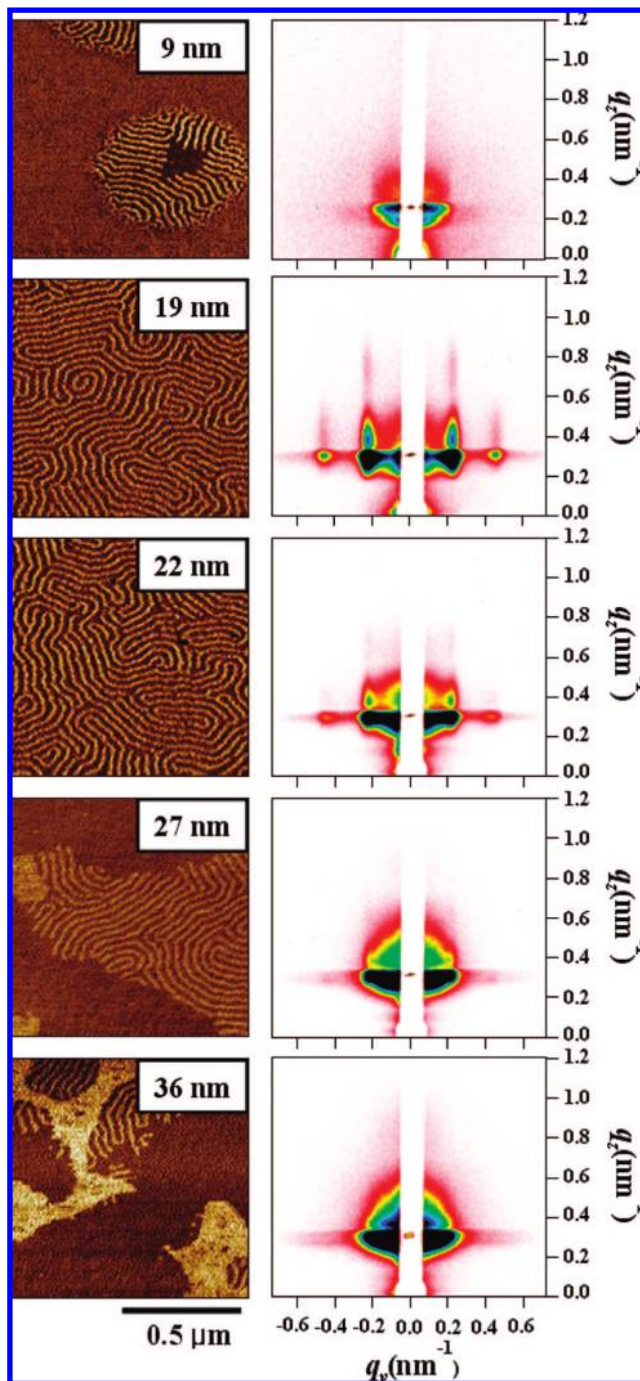
The maximum and minimum thicknesses for the perpendicular microdomain orientation of cylinder-forming PS-*b*-PMMA were consequently determined as a thickness window for the surfaces modified by the random copolymers with $X_{PS}$ ranging from 0.34 to 0.85. The SFM results on the surface morphologies and GISAXS results are summarized in Figure 5. When $X_{PS} < 0.48$, the microdomains were always oriented parallel to the film surface regardless of the film thicknesses. For R52 ($X_{PS} = 0.52$), the microdomains orient normal to the film surface for a very narrow thickness window of $32 \pm 1$ nm. With increasing $X_{PS}$, the thickness window increases and is largest when $X_{PS} = 0.64$ where a microdomain orientation normal to the surface is seen for film thicknesses from 13 to 42 nm (SEM image for film thickness of 42 nm in the inset of Figure 5) and then
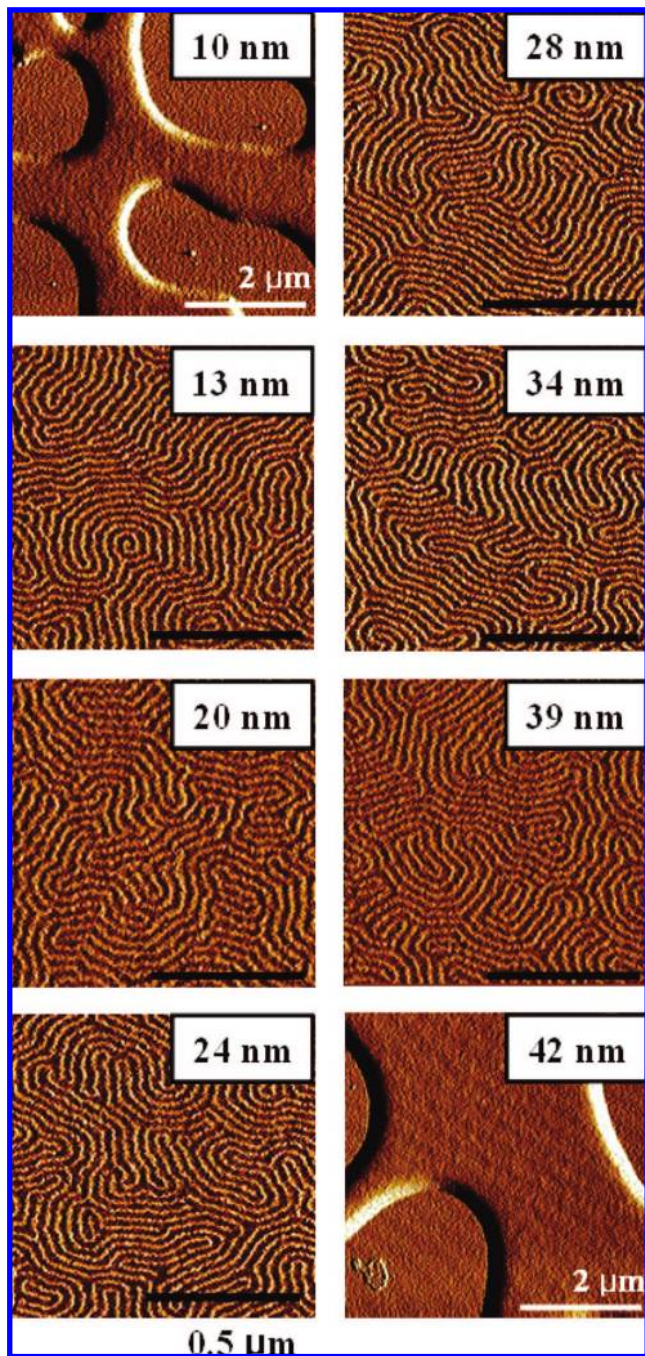
**Figure 6.** SFM phase images for thin films of lamella-forming PS-*b*-PMMA on the substrate modified by R55 (having a PS mole fraction of 0.55) at various film thicknesses of block copolymer after thermally annealing thin films at 170 °C for 24 h.



**Figure 7.** SFM phase images and two-dimensional GISAXS patterns at incident angle of 0.16° for thin films of lamella-forming PS-*b*-PMMA on the substrate modified by R64 at various film thicknesses of block copolymer after thermally annealing thin films at 170 °C for 24 h. To increase the scattering contrast, PMMA microdomains were removed from all thin film samples by UV exposure and subsequent rinsing with acetic acid.

decreases up to $X_{PS} = 0.72$ where the window is $33 \pm 2.5$ nm. When $X_{PS} > 0.78$, only a microdomain orientation parallel to the surface is again seen, regardless of the film thicknesses as is the case of the surface modified by R48. Consequently, for cylinder-forming PS-*b*-PMMA, when $X_{PS} = 0.64$ of random copolymer, an optimal condition for the balanced interfacial interactions is achieved.

A similar study was performed on PS-*b*-PMMA having lamellar microdomains. Figure 6 shows SFM phase images for thin films of block copolymer on R55 after thermally annealing thin films at 170 °C for 24 h under vacuum. When the film thickness is ~10 nm (or thinner), typical hole/island structures are seen while the microdomain orientation normal to the film surface is relegated to the edge of the hole/islands.[11] For film

thicknesses ranging from 13 to 39 nm on the surface modified by R55, the lamellar microdomains orient normal to the film surface. If the film thickness is greater than 42 nm, an hole/ island topography is seen, which is characteristic of an lamellar microdomain orientation parallel to the film surface. This change in orientation, when the interactions at both interfaces are balanced, as discussed by Walton et al. arises from a frustration of the lamellar microdomain morphology which gives rise to a stretching or compression of the chains in the block copolymer.[39]

Figure 7 shows SFM phase images and GISAXS patterns for thin films of lamella-forming PS-*b*-PMMA on R64, which
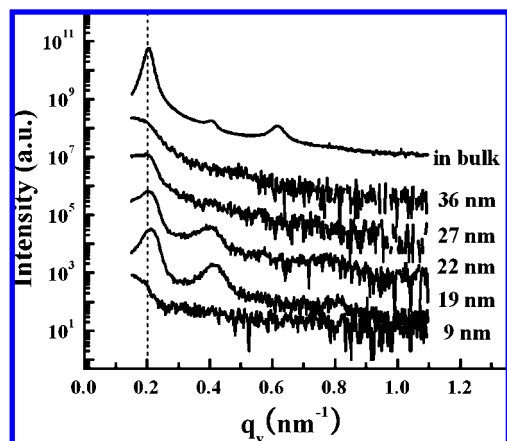
**Figure 8.** Intensity profiles scanned at constant $q_z = 0.254$ nm$^{-1}$ from Figure 7 as a function of $q_y$ at various film thicknesses of block copolymer and bulk state. A dashed line is drawn to compare the peak maxima.
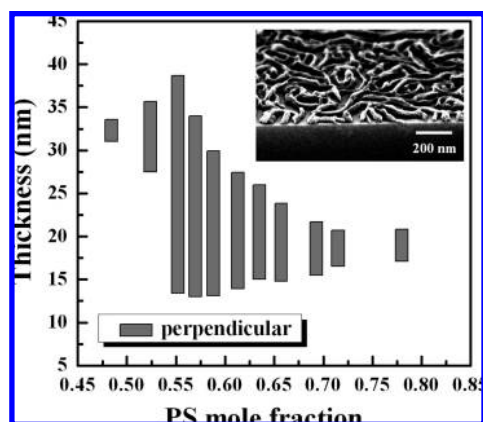


**Figure 9.** Thickness window for the perpendicular microdomain orientation of lamella-forming PS-*b*-PMMA on the substrates modified by various random copolymers composed of S and MMA. The cross-sectional SEM image was taken at a tilt angle of 55° for thin film with the maximum thickness of 39 nm on R55 (having a PS mole fraction of 0.55).

was found to be the optimal value of $X_{PS}$ to the balanced interfacial interactions for cylinder-forming PS-*b*-PMMA. Surface morphologies for thin films with thicknesses less than 9 nm and greater than 27 nm show an hole/island topography. When $X_{PS} = 0.64$, a narrower thickness window from 15 to 26 nm was found where the lamellar microdomains orient normal to the films surface, as shown in Figure 9. The GISAXS patterns for these thin films, as seen in Figure 7 for the film thicknesses of 19 and 22 nm, show a sharp first-order peak at $q_y = 0.214$ nm$^{-1}$ with higher-order peaks along constant $q_z = 0.254$ nm$^{-1}$ at scattering vector ratios of 1:2:3 relative to a first-order peak, corresponding to a lamellar microdomain oriented normal to the films surface.[40]

The intensity profiles from GISAXS patterns, scanned along $q_y$ direction at constant $q_z = 0.254$ nm$^{-1}$, are shown in Figure 8. First- and higher-order reflections are seen in thin films with thicknesses of 19 and 22 nm with a *d*-spacing of 29.4 nm, characteristic of lamellar microdomains oriented normal to the films surface. All the GISAXS patterns are in good agreement with the SFM phase images for thin films on R64 in terms of the size and orientations of the microdomains. It should be noted in this study that the *d*-spacing by $d = 2\pi/q_y^{max}$ in bulk state measured by SAXS is identical to that seen in thin films for cylinder-forming PS-*b*-PMMA, but *d*-spacing in bulk state for lamella-forming PS-*b*-PMMA is larger than that

observed in the thin films, as indicated in Figure 4 and Figure 8, respectively. The exact origin of this difference is not known, although this is presumably attributed to the reduced entropic penalty due to the perpendicular orientation of lamellar microdomains.

The thickness window for the perpendicular microdomain orientation of lamella-forming PS-*b*-PMMA is given in Figure 9 as a function of $X_{PS}$ of random copolymers anchored to the substrate. From these data, $X_{PS} = 0.55$ appears to be the optimal value of $X_{PS}$ to the balanced interfacial interactions since the perpendicular microdomain orientation persists over the broadest range of thicknesses, from 13 to 39 nm (SEM image for film thickness of 39 nm in the inset of Figure 9). The difference in optimal values of $X_{PS}$ between cylinder- and lamella-forming PS-*b*-PMMAs, 0.64 and 0.55, respectively, is noteworthy, suggesting that the optimal conditions for the balanced interfacial interactions depend on each microdomain structure of block copolymers. In addition, different from the thickness window for the perpendicular microdomain orientation of cylinder-forming PS-*b*-PMMA, the thickness window for lamella-forming PS-*b*-PMMA particularly shows the extensive range of $X_{PS}$ in the random copolymers ranging from 0.48 (R48) to 0.78 (R78) with each thickness dependence. This result indicates that the perpendicular orientation of lamellar microdomains is more entropically favorable by the equal sharing of microdomains on the substrates than that of cylindrical microdomains. Therefore, it is of great interest to investigate the composition effect of block copolymers for the perpendicular microdomain orientations, holding at the same microdomain structures, which is under study as a further topic.

## Summary

The microdomain orientation in thin films of cylinder- and lamella-forming PS-*b*-PMMAs was investigated as a function of the film thickness and the composition of P(S-*r*-MMA) anchored to the substrate, ranging from 0.34 to 0.85 of $X_{PS}$. From the dependence of the perpendicular microdomain orientation on film thickness around lattice period ($L_0$), the optimal values of $X_{PS}$ in the P(S-*r*-MMA) anchored to the substrate were 0.64 and 0.55 for PS-*b*-PMMA having cylindrical and lamellar microdomains, respectively. In addition, the thickness window over which the microdomain orientation normal to the film surface persisted was larger for the lamellar microdomain morphology, ranging extensively from 0.48 to 0.78 (in Figure 9). Taken together, these results clearly show that it is easier to orient lamellar, as compared to cylindrical, microdomains normal to the film surface. This study suggests a simple and informative guide to the desired microdomain orientation of PS-*b*-PMMA in fabrication of nanostructured thin films.

## References and Notes

(1) Mansky, P.; Harrison, C. K.; Chaikin, P. M.; Register, R. A.; Yao, N. *Appl. Phys. Lett.* **1996**, *68*, 2586.

(2) Park, C.; Cheng, J. Y.; Fasolka, M. J.; Mayes, A. M.; Ross, C. A.; Thomas, E. L.; De Rosa, C. *Appl. Phys. Lett.* **2001**, *79*, 848.

(3) Thurn-Albrecht, T.; Steiner, R.; DeRouchey, J.; Stafford, C. M.; Huang, E.; Bal, M.; Tuominen, M.; Hawker, C. J.; Russell, T. P. *Adv. Mater.* **2000**, *12*, 787.

(4) Thurn-Albrecht, T.; Schotter, J.; Kastle, G. A.; Emley, N.; Shibauchi, T.; Krusin-Elbaum, L.; Guarini, K.; Black, C. T.; Tuominen, M. T.; RussellT. P. *Science* **2000**, *290*, 2126.

(5) Yang, S. Y.; Ryu, I.; Kim, H. Y.; Kim, J. K.; Jang, S. K.; Russell, T. P. *Adv. Mater.* **2006**, *18*, 709.

(6) Holden, G.; Legge, N. R.; Schroeder, H. E.; Quirk, R. P. *Thermoplastic Elastomers*; Hanser: New York, 1987.

(7) Bates, F. S.; Fredrickson, G. H. *Annu. Rev. Phys. Chem.* **1990**, *41*, 525.

(8) Hamley, I. W. *The Physics of Block Copolymers*; Oxford University Press: New York, 1998.

(9) Singh, C.; Pickett, G. T.; Zhulina, E.; Balazs, A. C. *J. Phys. Chem. B* **1997**, *101*, 10614.

(10) Fasolka, M. J.; Banerjee, P.; Mayes, A. M.; Pickett, G.; Balazs, A. C. *Macromolecules* **2000**, *33*, 5702.

(11) Russell, T. P.; Coulon, G.; Deline, V. R.; Miller, D. C. *Macromolecules* **1989**, *22*, 4600.

(12) Russell, T. P.; Menelle, A.; Anastasiadis, S. H.; Satija, S. K.; Majkrzak, C. F. *Macromolecules* **1991**, *24*, 6263.

(13) Pickett, G. T.; Balazs, A. C. *Macromolecules* **1997**, *30*, 3097.

(14) Kim, H.-C.; Russell, T. P. *J. Polym. Sci., Part B: Polym. Phys.* **2001**, *39*, 663.

(15) Khanna, V.; Cochran, E. W.; Hexemer, A.; Stein, G. E.; Fredrickson, G. H.; Kramer, E. J.; Li, X.; Wang, J.; Hahn, S. F. *Macromolecules* **2006**, *39*, 9346.

(16) Bain, C. D.; Biebuyck, H. A.; Whitesides, G. M. *Langmuir* **1989**, *5*, 723.

(17) Peters, R. D.; Yang, X. M.; Kim, T. K.; Sohn, B. H.; Nealey, P. F. *Langmuir* **2000**, *16*, 4625.

(18) Guarini, K. W.; Black, C. T.; Yeung, S. H. I. *Adv. Mater.* **2002**, *14*, 1290.

(19) Jeong, U.; Ryu, D. Y.; Kho, D. H.; Kim, J. K.; Goldbach, J. T.; Kim, D. H.; Russell, T. P. *Adv. Mater.* **2004**, *16*, 533.

(20) Wang, H.; Djurisic, A. B.; Xie, M. H.; Chan, W. K.; Kutsay, O. *Thin Solid Films* **2005**, *488*, 329.

(21) Kitano, H.; Akasaka, S.; Inoue, T.; Chen, F.; Takenaka, M.; Hasegawa, H.; Yoshida, H.; Nagano, H. *Langmuir* **2007**, *23*, 6404.

(22) Huang, E.; Rockford, L.; Russell, T. P.; Hawker, C. J. *Nature (London)* **1998**, *395*, 757.

(23) Kim, S. O.; Solak, H. H.; Stoykovich, M. P.; Ferrier, N. J.; de Pablo, J. J.; Nealey, P. F. *Nature (London)* **2003**, *424*, 411.

(24) Huang, E.; Russell, T. P.; Harrison, C.; Chaikin, P. M.; Register, R. A.; Hawker, C. J.; Mays, J. *Macromolecules* **1998**, *31*, 7641.

(25) Ryu, D. Y.; Shin, K.; Drockenmuller, E.; Hawker, C. J.; Russell, T. P. *Science* **2005**, *308*, 236.

(26) Thurn-Albrecht, T.; DeRouchey, J.; Russell, T. P.; Jaeger, H. M. *Macromolecules* **2000**, *33*, 3250.

(27) Thurn-Albrecht, T.; DeRouchey, J.; Russell, T. P.; Kolb, R. *Macromolecules* **2002**, *35*, 8106.

(28) Kim, S. H.; Misner, M. J.; Xu, T.; Kimura, M.; Russell, T. P. *Adv. Mater.* **2004**, *16*, 226.

(29) Xuan, Y.; Peng, J.; Cui, L.; Wang, H.; Li, B.; Han, Y. *Macromolecules* **2004**, *37*, 7301.

(30) In, I.; La, Y. H.; Park, S. M.; Nealey, P. F.; Gopalan, P. *Langmuir* **2006**, *22*, 7855.

(31) Han, E.; In, I.; Park, S.-M.; La, Y.-H.; Wang, Y.; Nealey, P. F.; Gopalan, P. *Adv. Mater.* **2007**, *19*, 4448.

(32) Ryu, D. Y.; Wang, J. Y.; Lavery, K. A.; Drockenmuller, E.; Satija, S. K.; Hawker, C. J.; Russell, T. P. *Macromolecules* **2007**, *40*, 4296.

(33) Mansky, P.; Liu, Y.; Huang, E.; Russell, T. P.; Hawker, C. *Science* **1997**, *275*, 1458.

(34) Tsui, O. K. C.; Russell, T. P.; Hawker, C. J. *Macromolecules* **2001**, *34*, 5535.

(35) Potemkin, I. I. *Macromolecules* **2004**, *37*, 3505.

(36) Anastasiadis, S. H.; Gancarz, I.; Koberstein, J. T. *Macromolecules* **1988**, *21*, 2980.

(37) He, J.; Tangirala, R.; Emrick, T.; Russell, T. P.; Böker, A.; Li, X.; Wang, J. *Adv. Mater.* **2007**, *19*, 381.

(38) Yoon, J.; Yang, S. Y.; Lee, B.; Joo, W.; Heo, K.; Kim, J. K.; Ree, M. *J. Appl. Crystallogr.* **2007**, *40*, 305.

(39) Walton, D. G.; Kellogg, G. J.; Mayes, A. M.; Lambooy, P.; Russell, T. P. *Macromolecules* **1994**, *27*, 6225.

(40) Busch, P.; Posselt, D.; Smilgies, D. M.; Rauscher, M.; Papadakis, C. M. *Macromolecules* **2007**, *40*, 630.